JOURNAL OF MATERIALS SCIENCE 27 (1992) 825–838

Effect of heat treatment in air on the structure and properties of barium osumilite reinforced with Nicalon fibres

S. M. BLEAY, V. D. SCOTT
School of Materials Science, University of Bath, Calverton Down, Bath BA2 7AY, UK

Microstructural studies have been carried out on glass-ceramic matrix composites, consisting of barium osumilite reinforced with Nicalon fibres, which have been subjected to heat treatment in air in the range 600–1100 °C. Parallel studies have involved the measurement of the friction stress between fibre and matrix and the flexural strength of the composite. The matrix was shown to consist of barium osumilite, hexacelsian, mullite and a silica-rich glass, the thermal mismatch of these different phases leading to the development of appreciable strains. Whilst high-temperature treatments caused the formation of voids due to flow of the glassy phase, the major factor controlling the mechanical properties of the composite was the fibre/matrix interface. A change in microstructure, from a weak carbon-rich interface to one where the fibre and matrix were strongly bonded together by a silica layer, was thus reflected in an increase in the interfacial friction stress and a change in fracture behaviour from one showing fibre pull-out and delamination to one with brittle characteristics.

1. Introduction

The principle of using ceramic fibre reinforcements in systems such as Pyrex/carbon [1], Pyrex/Nicalon [2] and lithium aluminosilicate/Nicalon [3] is well documented. The underlying principle of the fibre reinforcement is that its higher failure strain allows the matrix to fracture several times before final composite failure, and that any cracks propagating through the matrix can be deflected around the fibres to produce a controlled fracture rather than the catastrophic brittle failure normally associated with monolithic materials.

Barium osumilite is a glass-ceramic formulation developed by Brennan *et al.* [4], and believed to be suitable for high-temperature composite applications. As a consequence, there have been investigations of this system as a matrix for SiC whiskers including its mechanical behaviour [5] and thermal diffusivity properties [6]. More recently, work has been focused on reinforced barium osumilite with Nicalon fibres [7], studying the effect of heat treatment on the fibre/matrix interface strength and the resultant fracture behaviour.

In this paper, we present a detailed microstructural study of the barium osumilite/Nicalon system, and of the subsequent changes in microstructure brought about by heat treatment. The effects of heat treatment on fibre/matrix interfacial stress, composite flexural strength and resultant fractography are also evaluated and the data correlated with the microstructural evidence.

2. Experimental procedure

2.1. Materials

The composite material consisted of a glass-ceramic based on barium osumilite which was reinforced with Nicalon fibres. It was manufactured by hot-pressing at ~ 1500 °C [4] and supplied as unidirectional plate of average thickness 1.8 mm and $[0°/90°]_{3s}$ cross-ply plate of ~ 2.5 mm thickness.

2.2. Mechanical testing

Samples 50 mm × 10 mm were cut from the plates using a resin-bonded diamond saw at low speed. The size was dictated by the availability of the raw material and the constraints of the test, giving span:thickness ratios of 20:1 and 15:1 for unidirectional and cross-ply material, respectively. The cut surfaces were then smoothed using 240 grit SiC paper. Testing was carried out in three-point flexure on an Instron model 1195 at a crosshead speed of 0.5 mm min^{-1}. Specimens were heated in air for 60 h at temperatures of 600, 800, 1000 and 1100 °C and air cooled.

2.3. Interface friction measurements

Values of interfacial friction stress were obtained using the microindentation technique developed by Marshall and Evans [8]. A polished transverse section of composite was first prepared and the centre of an

0022–2461/92 $03.00 + .12 © *1992 Chapman & Hall*

individual fibre was then loaded with a Vickers pyramidal microindentor until the fibre/matrix interfacial bond was broken and the fibre slid within the matrix. When the applied load depressed the fibre to the extent that the indentor contacted the matrix, the interfacial friction stress was calculated from the size of indent in the fibre and the surrounding matrix, using the formula given [8]. A LECO M-400 hardness tester was used for these measurements, the load applied ranging from 1–2 N.

Data were recorded on fibres within the interior of the composite plate and the outermost (~ 100 μm) surface regions for the different heat-treatment conditions.

2.4. Microstructural examination

Sections taken from unidirectional and cross-ply plate before and after heat treatments were mounted in "Epofix" cold-curing resin and ground planar using a diamond wheel with water lubricant. Three further polishing stages were required to produce the final surface, using Buehler Metlap wheels of decreasing hardness sprayed with diamond slurries of particle size 9, 6 and 1 μm, respectively. Polished sections were also prepared through fracture surfaces of tested samples.

Optical microscopy was performed on a Zeiss ICM 405 optical microscope fitted with Nomarski interference contrast. Prior to examination in the scanning electron microscope (SEM), polished samples were coated with a thin conducting layer of carbon. A JEOL 35C SEM was used which was fitted with backscattered electron imaging (BEI) and a Link AN 10000 energy dispersive X-ray spectrometer (EDS) for compositional analysis of microstructural features. SEM was also carried out on fracture surfaces of samples broken in flexure, and again a thin conductive coating was applied to the specimen surface before examination.

Thin foils for transmission electron microscopy (TEM) were prepared by drilling 3 mm discs from the composite with a diamond-tipped coring drill. Each disc was ground to a thickness of ~ 300 μm on 400 grit SiC paper, then "dimpled" in a VCR Model D500 to leave a central specimen thickness of ~ 20 μm. Final thinning was accomplished by argon-ion bombardment in a Gatan Duomill operating at 5 kV. An argon-beam incidence angle of 15° was first used and, when a hole was formed in the disc, the incidence angle was reduced to 8° and thinning continued to extend the area for analysis. Examination of foils was carried out in a Jeol 2000FX microscope fitted with a Link AN 10000 EDS facility capable of ultra-light element ($Z > 4$) detection. The TEM system was operated in the bright-field, selected-area diffraction (SAD) and EDS modes.

Finally, sections of cross-ply plate, before and after heating in air at 1100 °C for 60 h, were ground into powder using a pestle and mortar, and examined in a Philips PW 1820 X-ray diffractometer through the Bragg angle, θ, range $5° < \theta < 35°$.

3. Results

3.1. Mechanical testing

Load versus deflection curves for unidirectional material, as recorded in flexural tests, are given in Fig. 1. Considering first the as-received material (Curve a), the initial part of the curve shows proportionality between load and deflection. The load maximum was reached at 250 N (~ 320 MPa), and the load decrease which followed was characteristic of a slow, relatively controlled damage process. Even after the test was terminated, the specimen was able to sustain some measure of load-bearing capacity (approximately one-quarter of the maximum value reached). Similar load versus deflection characteristics were recorded in tests on samples heat treated at 600 and 800 °C (Curves b and c). The maximum loads reached were lower, however, at ~ 200 N (250 MPa), and a discontinuity (arrowed) was seen at ~ 60 N (~ 100 MPa) which was believed to indicate the onset of matrix cracking. The discontinuity was not so evident in the curve from as-received material, as the matrix of the particular composite plate was better consolidated with fewer flaws. In contrast, a specimen tested after heat treatment at 1000 °C (Curve d) exhibited brittle characteristics and fractured catastrophically at a load of ~ 75 N (~ 120 MPa), well below the value reached in the above tests. After treatment at 1100 °C, however, the behaviour (Curve e) more closely resembled that associated with slow controlled crack growth, whilst the maximum load that the material was now able to sustain reached ~ 140 N.

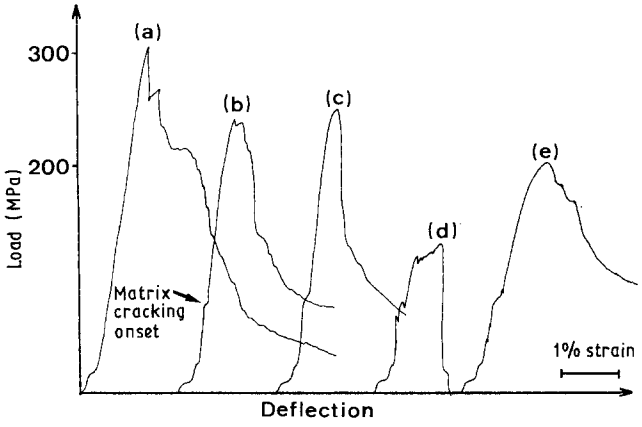

Figure 1 Load versus deflection curves for heat-treated unidirectional specimens.

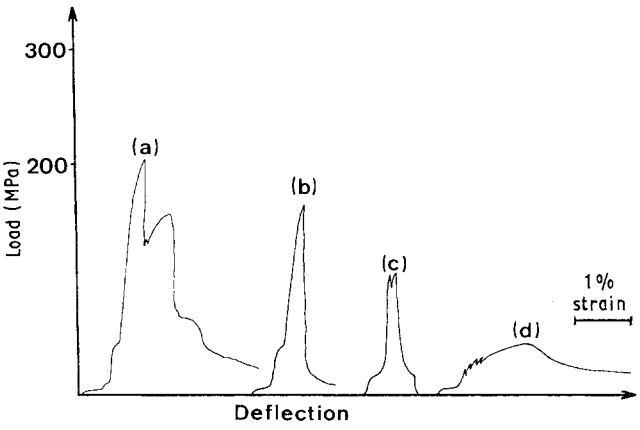

Figure 2 Load versus deflection curves for heat-treated cross-ply specimens.

Tests carried out on 600 °C HT cross-ply plate, Fig. 2 (Curve a) indicated a strength of ~ 280 ± 30 MPa. Again a discontinuity in the initial part of the curve was noted at around 50 N, whilst the series of the maxima may be indicative of failure of successive 0° plies as the crack propagates. Specimen failure characteristics reflected relatively slow and controlled cracking, with the sample still able to sustain some load after a strain of ~ 3%. Brittle characteristics were observed after treatment at 800 °C, as evinced by the sharp load drop at around 1% (Curve b) and were even more apparent after heating at 1000 °C (Curve c). Treatment at 1100 °C failed to restore the strength of the material, in contrast to the corresponding unidirectional plate, although the failure was not entirely catastrophic (Curve d).

The results of the flexural tests are compiled in Table I, and the effect of heat treatment on the two types of composite plate is plotted graphically in Fig. 3. It should be remarked that only two tests were carried out for each heat-treatment condition and so it was not possible to carry out detailed statistical analysis of the measurements, although estimates of reproducibility gave it as approximately 10% of relative.

With most of the samples tested, the crack nucleated on that side of the specimen which experienced a tensile stress. However, with unidirectional samples in the as-received condition and after treatment at 600 or 800 °C, it was noted that failure occurred on the compressive face, apparently by large-scale buckling and delamination in the interior of the material.

TABLE I Mechanical test results for Nicalon/BMAS composites

Heat-treatment temperature (°C)	Flexural strength (MPa) and failure mode			
	Unidirectional plate		Cross-ply plate	
	1	2	1	2
As-received		320 ± 80 Compressive	–	–
600	230 Compressive	250 Compressive	283 Tensile	197 Tensile
800	275 Compressive	240 Compressive	190 Tensile	205 Tensile
1000	140 Tensile	95 Tensile	115 Tensile	42 Tensile
1100	230 Tensile	225 Tensile	105 Tensile	72 Tensile

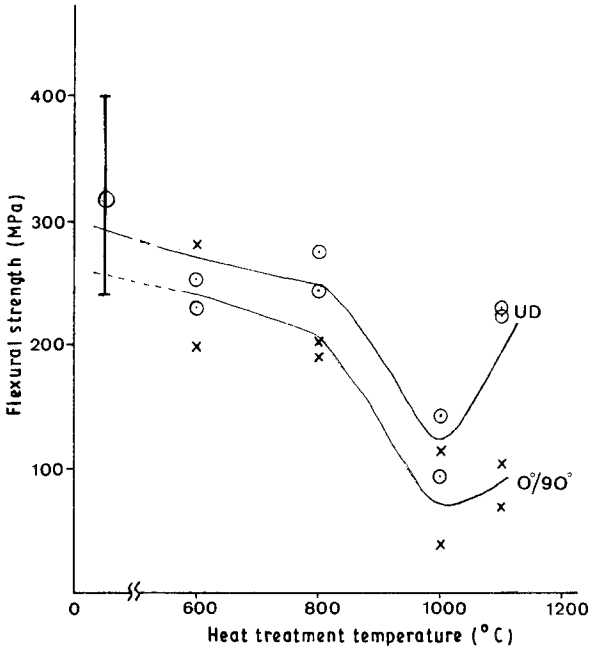

Figure 3 Graph of flexural strength versus heat-treatment temperature for (○) unidirectional and (×) cross-ply specimens.

3.2. Interface friction measurements

Values of interfacial friction stress for the interior and for the surface regions of the composite plates are given in Table II and plotted against temperature in Fig. 4a and b, for unidirectional and cross-ply material, respectively. Each "interior" point is an average of 20 readings and each "surface" point an average of 10 measurements. The results show that heat treatment had significantly affected interfacial friction stress in

TABLE II Interfacial friction stress values for heat-treated Nicalon/BMAS composites

Heat-treatment temperature (°C)	Interfacial friction stress (MPa)			
	Unidirectional plate		Cross-ply plate	
	Bulk	Edge	Bulk	Edge
As-received	4.4 ± 0.8	3.5 ± 0.7	–	–
600	3.9 ± 1.6	4.8 ± 2.1	5.9 ± 2.4	6.5 ± 2.0
800	6.7 ± 2.9	6.4 ± 1.5	7.7 ± 1.2	7.8 ± 1.8
1000	35.2 ± 24.7	46.4 ± 19.3	22.2 ± 13.0	44.4 ± 14.4
1100	4.4 ± 0.8	71.4 ± 15.0	50.9 ± 31.2	52.9 ± 11.5

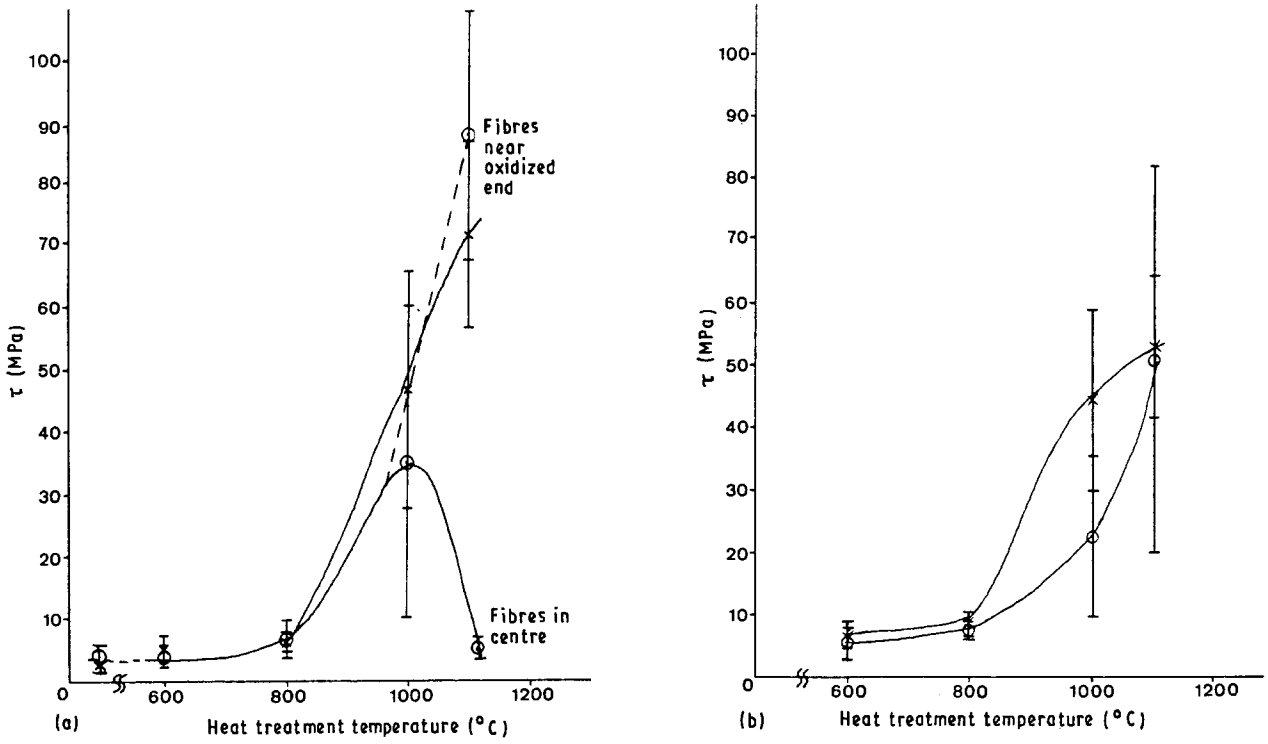

Figure 4 Graphs of interfacial friction stress, τ, versus heat-treatment temperature for (a) unidirectional specimens, and (b) crossply specimens (×) Edge, (⊙) interior.

both unidirectional and cross-ply plates, the stress increasing progressively with increase in temperature. In samples given the 1000 °C heat treatment, the interfacial friction stress was found to be significantly higher in surface regions, compared with the interior of the sample. Such differences were also found in the 1100 °C heat-treated sample, although in this case the interfacial friction stress values in the interior were even lower, close to these recorded in as-received specimens.

3.3. Microstructural examination

3.3.1. As-received composite

An X-ray diffraction (XRD) trace obtained from powdered composite is shown in Fig. 5. Three crystalline phases were identified from the data: barium osumilite, $BaMg_2Al_3(Si_9Al_3O_{30})$; hexacelsian, $BaAl_2Si_2O_8$; mullite, $Al_6Si_2O_{13}$. The first two phases have hexagonal structures and the latter is orthorhombic; measured d-spacings and indexed diffractions are listed in Table III. The unit cell dimensions were calculated to be: barium osumilite $a_o = 1.0119$ nm, $c_o = 1.4302$ nm; hexacelsian $a_o = 0.5311$ nm, $c_o = 0.7767$ nm; mullite $a_o = 0.7583$ nm, $b_o = 0.7639$ nm, $c_o = 0.2891$ nm. The values agree closely with published data: barium osumilite $a_o = 1.016$ nm, $c_o = 1.436$ nm [9]; hexacelsian $a_o = 0.5313$ nm, $c_o = 0.7805$ nm, [10]; mullite $a_o = 0.754\,56$ nm, $b_o = 0.768\,98$ nm, $c_o = 0.288\,42$ nm [11]. It should be noted that in Table III diffractions which accord with the hexagonal structure $c/a = 1.413$, such as 1 0 2 and 2 1 3, have been attributed to barium osumilite, although they were not listed in Reference 9.

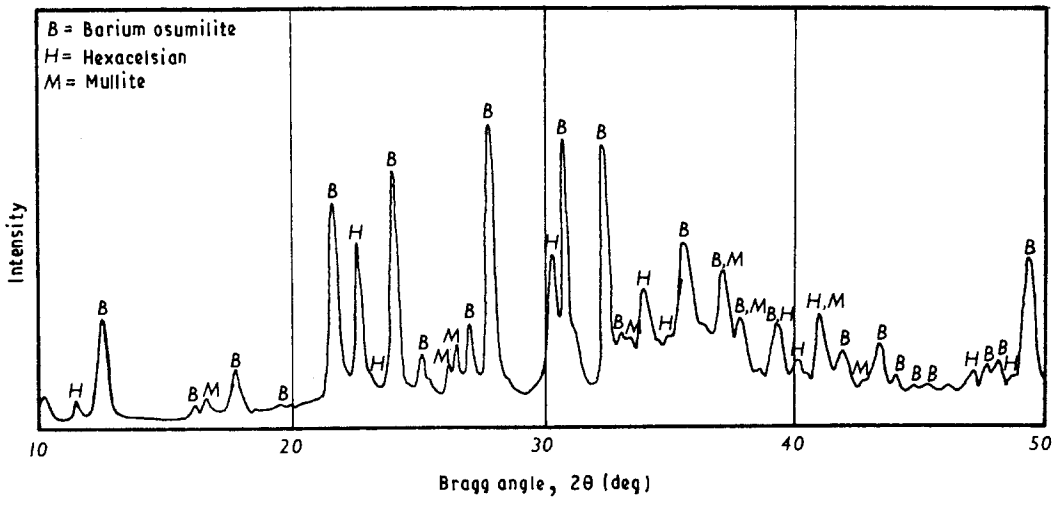

Figure 5 X-ray diffraction spectrum from powdered as-received composite.

TABLE III X-ray diffraction measurements

d-spacing (nm)	ASTM 16-402 barium osumilite	ASTM 12-726 hexacelsian	ASTM 15-776 mullite
0.7767	–	001	–
0.7151	002	–	–
0.5545	102[a]	–	–
0.5382	–	–	110
0.5057	110	–	–
0.4130	112	–	–
0.3954	–	101	–
0.3876	–	002	–
0.3737	202	–	–
0.3578	004	–	–
0.3421	–	–	120
0.3386	–	–	210
0.3312	120	–	–
0.3227	121	–	–
0.2967	–	102	–
0.2921	300	–	–
0.2891	–	–	001
0.2771	204	–	–
0.2721	213[a]	–	–
0.2702	–	–	220
0.2650	–	110	–
0.2590	–	003	–
0.2546	–	–	111
0.2530	220	–	–
0.2430	130	–	130
0.2386	006	–	310
0.2300	132	200	021
0.2259	–	103	–
0.2206	–	201	121
0.2163	313[a]	–	–
0.2118	–	–	230
0.2096	402[a]	–	–
0.2066	224	–	–
0.2009	314	–	–
0.1945	–	004	–
0.1896	410[a]	–	–
0.1852	315, 412[a]	113	–

[a] Not reported but could arise in a hexagonal structure with this *c/a* ratio.

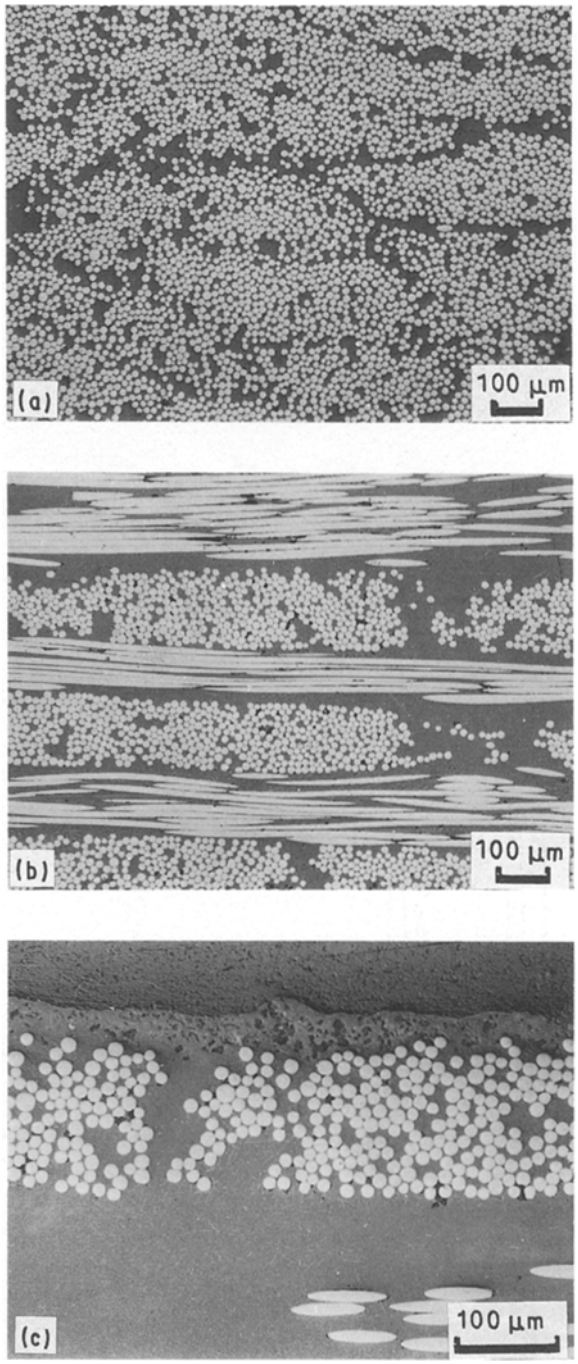

Figure 6 Optical micrographs of (a) unidirectional plate, polished section, (b) cross-ply plate, polished section, (c) cross-ply plate, polished section of surface region.

Optical microscopy, Fig. 6a, shows a fairly uniform distribution of fibres, ~ 15 μm diameter, with a few per cent by volume of pores but little sign of microcracks. In the cross-ply plate, Fig. 6b, there were more matrix-rich regions. From micrographs such as these it was estimated that the fibre volume fraction was 0.49 for unidirectional plate and 0.45 for cross-ply. The surface regions (some 50 μm) of plates appeared, however, to be of poor quality with an absence of fibres and a high degree of porosity, Fig. 6c.

The multi-phased structure of the matrix of the composite plate is readily revealed in the SEM by means of the BEI facility, Fig. 7a. The phases of lighter contrast have a high mean atomic number and the darker phases a low mean atomic number. Fig. 7b, an EDS trace from the continuous, medium contrast phase, shows the presence of substantial amounts of oxygen, aluminium, silicon and barium, together with a smaller concentration of magnesium. The data accord with the composition of barium osumilite, see Table IV. The angular particles of lighter phase, up to ~ 5 μm in size, were also found to be rich in oxygen, aluminium, silicon and barium, and whilst the barium level was higher than in barium osumilite, the aluminium content was less, Fig. 7c; these findings confirm that the lighter phase was hexacelsian, see Table IV. Turning now to the darker phase, EDS results, Fig. 7d, showed that it consisted of oxygen, aluminium and silicon; the much higher aluminium level compared with silicon indicating that it is mullite, Table IV; the small barium and magnesium peaks in the spectrum are probably due to electron excitation of surrounding matrix regions. From detailed studies of BEI pictures such as Fig. 7a, it was estimated that the barium osumilite, hexacelsian and mullite were present in the

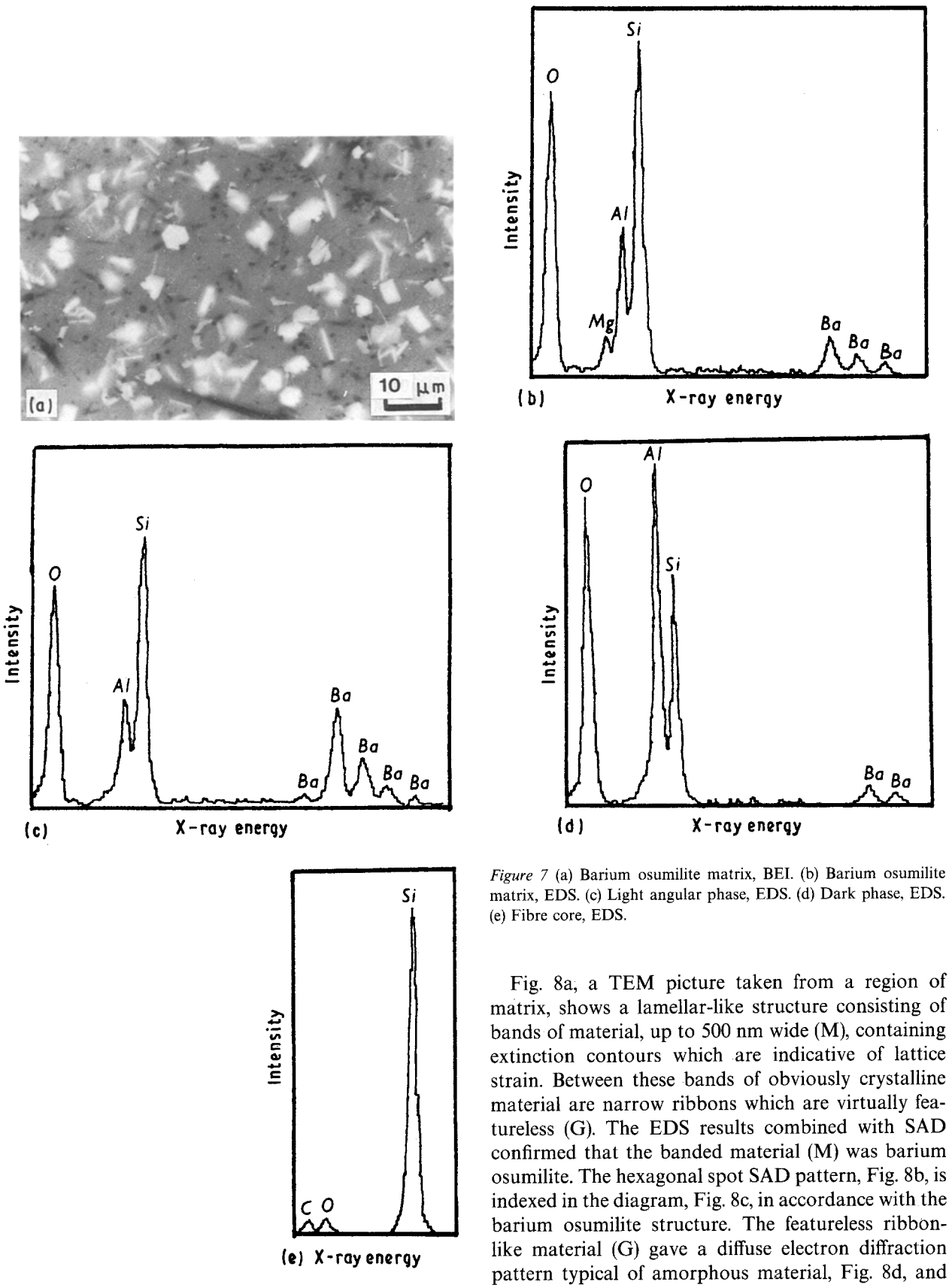

Figure 7 (a) Barium osumilite matrix, BEI. (b) Barium osumilite matrix, EDS. (c) Light angular phase, EDS. (d) Dark phase, EDS. (e) Fibre core, EDS.

proportions 6:2:1. The fourth EDS trace in this series was obtained from the centre of the fibre, and it shows the presence of oxygen as well as silicon and carbon, Fig. 7e. The data indicate that the Nicalon fibre contains ~ 8 wt % O and ~ 33 wt % C in accord with previous findings [12], the relatively low intensity of the carbon peak being due to high absorption of carbon X-rays in silicon carbide.

Fig. 8a, a TEM picture taken from a region of matrix, shows a lamellar-like structure consisting of bands of material, up to 500 nm wide (M), containing extinction contours which are indicative of lattice strain. Between these bands of obviously crystalline material are narrow ribbons which are virtually featureless (G). The EDS results combined with SAD confirmed that the banded material (M) was barium osumilite. The hexagonal spot SAD pattern, Fig. 8b, is indexed in the diagram, Fig. 8c, in accordance with the barium osumilite structure. The featureless ribbon-like material (G) gave a diffuse electron diffraction pattern typical of amorphous material, Fig. 8d, and was found to contain mainly oxygen and silicon, with small amounts of barium (~ 5 wt %), aluminium (~ 2 wt %) and magnesium (~ 1 wt %), Fig. 8e. Also visible is a large particle (H) in a state of strain which was identified as hexacelsian.

Another region of the foil, seen at higher magnification in Fig. 9a, shows two phases which have been labelled A and B. Phase A gave an EDS spectrum which accorded with mullite, as did the SAD spot pattern, Fig. 9b, although not completely indexible,

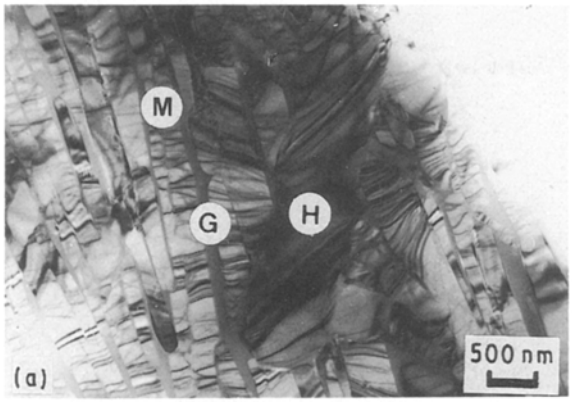

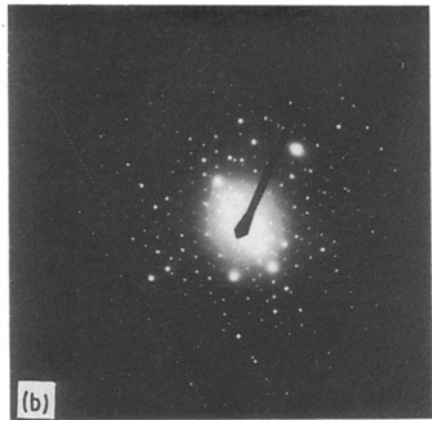

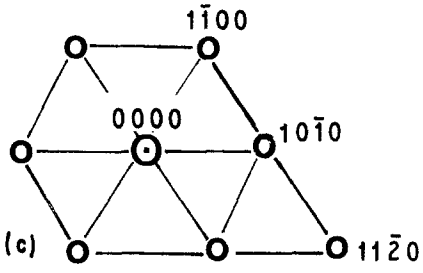

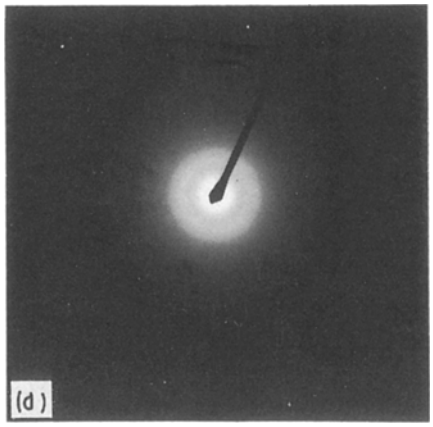

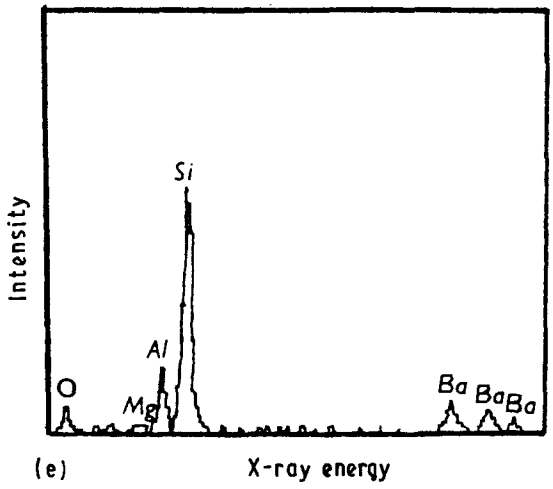

Figure 8 (a) Barium osumilite matrix and second-phase particle, TEM. (b) Barium osumilite phase, SAD. (c) Indexed SAD pattern. (d) Amorphous phase, SAD. (e) Amorphous phase, EDS.

Fig. 9c. The composition of Phase B corresponded to hexacelsian as did the electron diffraction analysis, Fig. 9d and e. Using EDS and SAD, the surrounding material was confirmed as barium osumilite.

A TEM picture of the fibre/matrix interface is shown in Fig. 10a. A reacted zone of material (I), ~ 50 nm wide and more electron transparent than the rest, is visible between the fibre and the matrix. EDS analysis of this interface zone is illustrated in Fig. 10b. EDS from fibres and matrix regions are not shown but were similar to Fig. 7b and e, respectively. Comparison of these data thus indicated that the reaction zone at the interface was enriched with carbon. Below the surface zone, the fibre composition was found to be slightly enriched in barium (~ 3 wt %) aluminium (~ 5 wt %) and magnesium (~ 1 wt %) up to a depth of several 100 nm.

3.3.2. Effect of heat treatment

The XRD pattern from the specimen heated in air at 1100 °C for 60 h showed the same phases present in the same proportions as for as-received material, indicating that the matrix was stable under these heat-treatment conditions.

SEM studies demonstrated that the surface of the composite plate was little affected by heat treatment at temperatures up to 1000 °C, Fig. 11a showing the porous stippled appearance characteristic of the as-received condition. After treatment at 1100 °C, however, the extrusion of a low melting point phase containing crystalline particles occurred, Fig. 11b.

The polished section of cross-ply composite heated at 1100 °C, Fig. 12, shows voidage within the matrix, which is probably associated with the ejection of a liquid phase or formation of volatiles, but little evidence of microcracking was observed. An SEM picture of this area, Fig. 13a, reveals the presence of a lighter diffusion zone, ~ 2 μm thick, in the surface regions of each fibre, the small voids which are visible marking the position of the original fibre/matrix interface. EDS, Fig. 13b, shows the diffusion zone to contain all the elements found in the matrix (oxygen, magnesium, aluminium, silicon and barium, see Fig. 7b) together with those comprising the fibre core (carbon, oxygen and silicon, see Fig. 7e). Such a band was also observed in polished sections of as-received specimens.

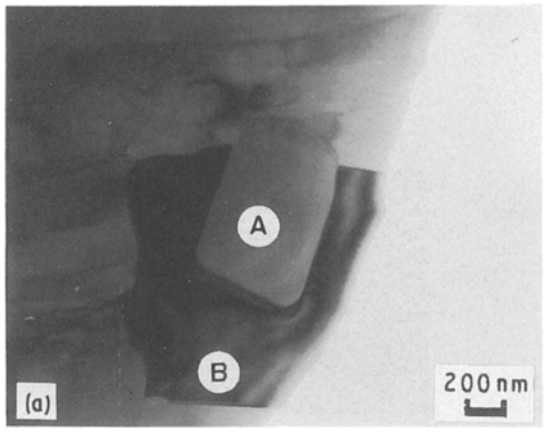

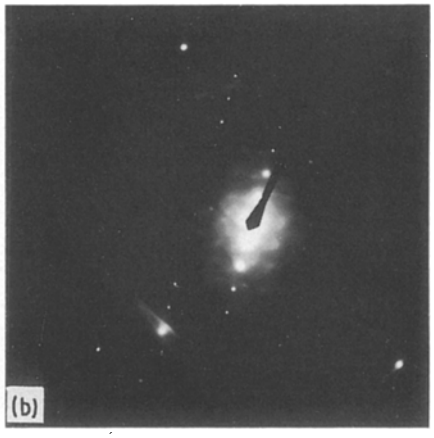

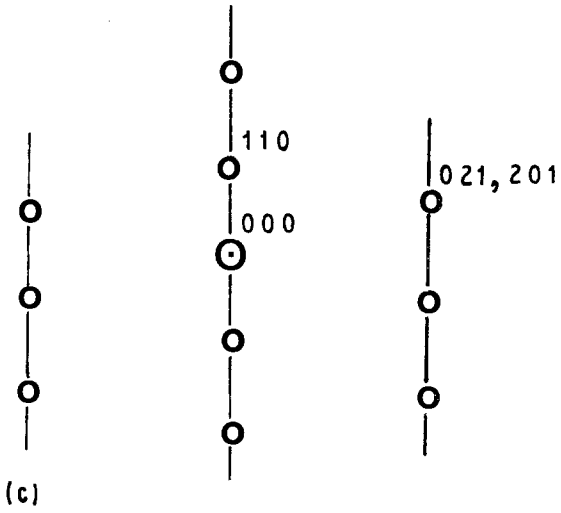

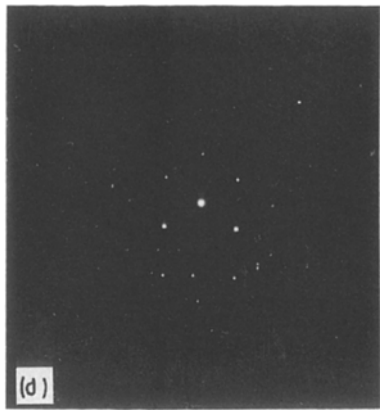

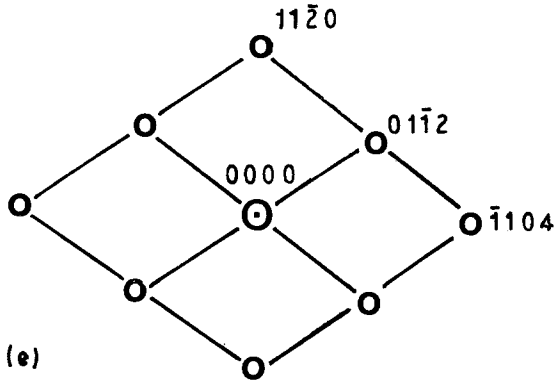

Figure 9 (a) Duplex particle in matrix, TEM. (b) Mullite phase, SAD. (c) Indexed SAD pattern. (d) Hexacelsian phase, SAD. (e) Indexed SAD pattern.

TEM studies revealed that little microstructural change had taken place at the fibre/matrix interface after heat treatment at 600 °C. After heating at 800 °C, however, the interface zone had undergone a change in appearance, voids being formed and also "bridges" of material between matrix and fibres, Fig. 14.

Changes in interface microstructure were even more extensive after treatment at 1100 °C. Fig. 15a is a TEM

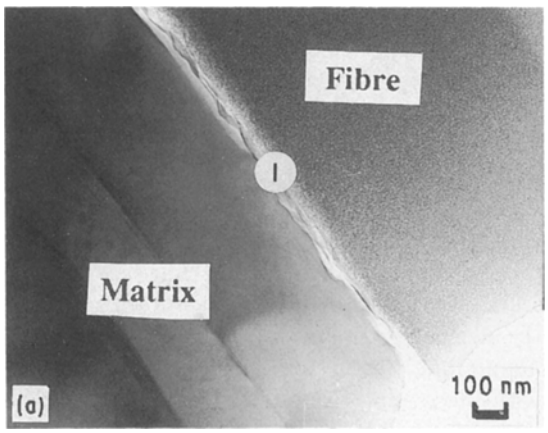

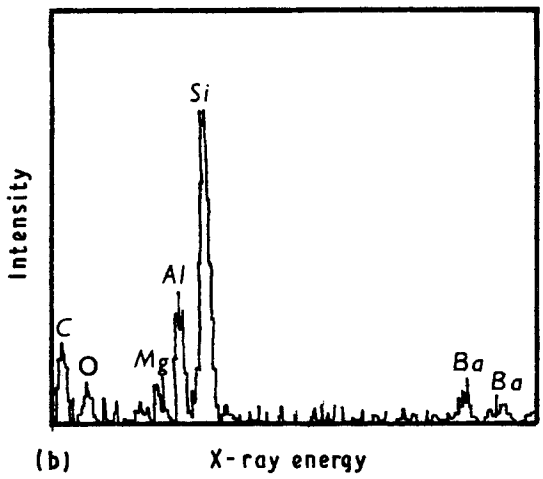

Figure 10 (a) As-received plate, fibre/matrix interface, TEM. (b) Interface, EDS.

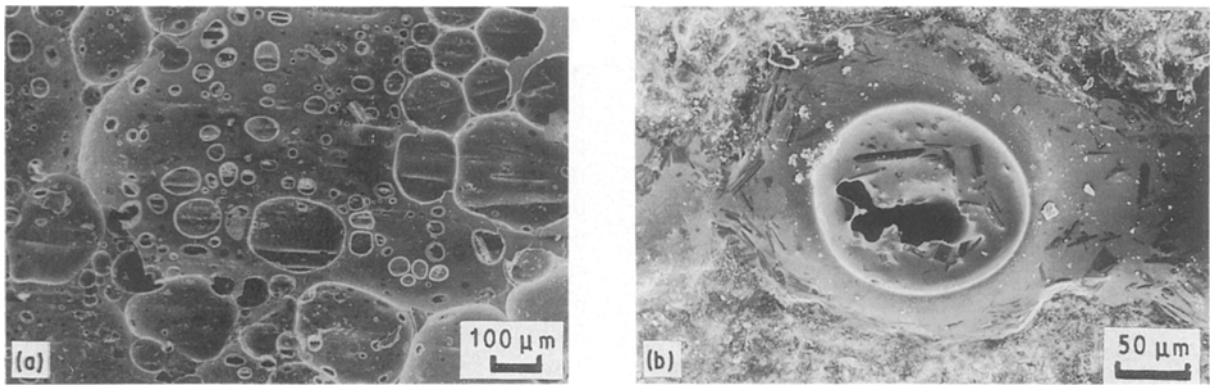

Figure 11 Scannning electron micrographs of (a) as-received plate, (b) 1100 °C HT plate.

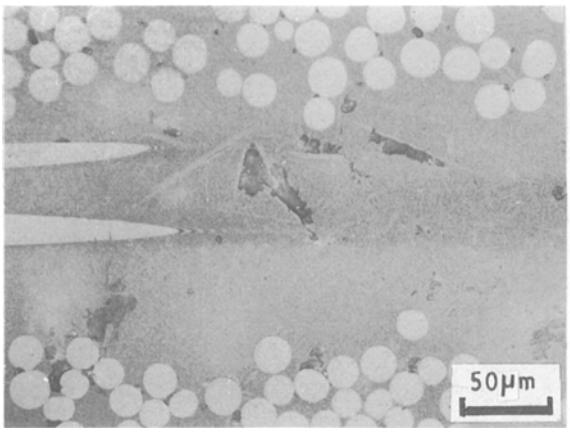

Figure 12 Optical micrograph of a polished section of 1100 °C HT cross-ply plate.

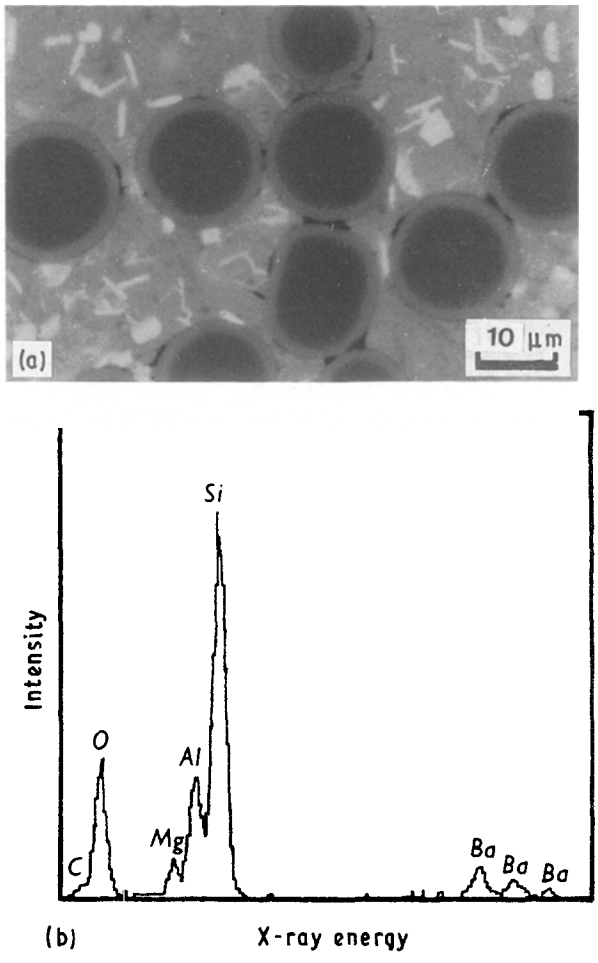

Figure 13 (a) Nicalon fibres in barium osumilite matrix, BEI. (b) Light surface zone, EDS.

picture taken from a matrix region separating two fibres. The matrix contains a large crack which may have arisen during preparation of the specimen foil. The original fibre/matrix interfaces have been labelled I_1 and I_2 and each has a featureless zone, ~ 200 nm thick, extending into the adjacent fibres. The zones, labelled Z_1 and Z_2 in the micrograph were found to be amorphous and to contain mainly silicon and oxygen with a little magnesium, aluminium and barium, Fig. 15b. The regions of fibre marked had compositions similar to that of the light diffusion zone found in the outer 2 µm layer of fibre, as pictured in Fig. 13a and subsequently shown in the EDS trace (Fig. 13b) to contain the matrix elements barium, aluminium and magnesium. The region of matrix sandwiched between the two fibres was found to contain more magnesium (~ 20 wt %), than the original matrix but less barium (~ 2 wt %), Fig. 15c. The porosity present at the fibre/matrix interface results from formation of voids during oxidation of the fibre and the original interfacial carbon layer.

Fig. 16a–c were taken from polished sections through the fracture face of cross-ply specimens tested in three-point bending. Fracture of the specimen heat treated at 600 °C, Fig. 16a, is accompanied by extensive fibre pull-out in the 0° plies and widespread delamination, the delaminating cracks propagating at angles of 10°–20° to the fibre axis. Fracture of the 800 °C treated specimen, Fig. 16b, shows shorter fibre pull-out in the 0° plies and crack propagation across the 90° plies is generally perpendicular to the fibre axis, apart from delamination in the centre ply. Treatment at 1000 °C resulted in much more brittle characteristics with fibre pull-out being virtually non-existent, Fig. 16c. Some fibre pull-out was observed in the interior of the specimen given the 1100 °C heat treatment, as evinced in the SEM picture of the fracture surface, Fig. 16d.

Similar trends were observed when testing unidirectional plates, i.e. as-received, 600- and 800 °C-treated samples showed failure by extensive delamination of

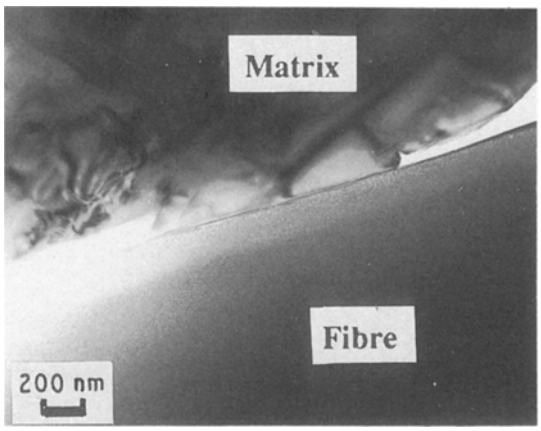

Figure 14 Transmission electron micrograph of an 800 °C HT plate, fibre/matrix interface.

the compressive surface, Fig. 17a and b, whilst samples heated at 1000 °C exhibited brittle, planar fracture surfaces with the crack propagating perpendicular to the fibre axis, Fig. 17c. In the interior of the 1100 °C-treated specimen, fibre pull-out was again observed, Fig. 17d.

4. Discussion

4.1. Microstructure and properties of as-received composites

The composite plates were almost fully dense apart from regions near the edge (~ 100 μm for unidirectional material and ~ 50 μm for cross-ply) where porosity and fibre degradation were present. These surface defects are believed to be associated with the production of volatile constituents during the manufacturing processes, and seemed to have little effect on overall mechanical properties in most cases, but may have been responsible for the compressive failure mode of unidirectional plates heated at temperatures below 800 °C. Fibres in the composites were fairly uniformly distributed, with volume fractions of 0.49 and 0.45 for unidirectional plate and cross-ply, respectively. The matrix of the composite was free from microcracks and contained four phases: barium osumilite, hexacelsian, mullite and a silica-rich glass. Based upon SEM and TEM observations, the amount of each phase present was estimated to be (vol %) $> 60 \pm 5$, 20 ± 5, 10 ± 5 and $< 10 \pm 5$, respectively, Table IV.

A distinctive feature of the microstructure of the matrix material was the appreciable lattice strain present in both barium osumilite and hexacelsian phases, as clearly evinced by the contrast effects revealed in the thin-foil TEM studies. Such strains are to be expected when cooling this multi-phased structure from the high temperature used in manufacture (~ 1500 °C) because the thermal expansion coefficients of the constituents differ considerably, ranging from $1.7 \times 10^{-6}\,K^{-1}$ for barium osumilite, through $4.5 \times 10^{-6}\,K^{-1}$ for mullite, to $8 \times 10^{-6}\,K^{-1}$ for hexacelsian, and $\sim 5 \times 10^{-6}\,K^{-1}$ for the glass (as deduced from published data for similar high silica-containing glasses). Of course, in the initial stages of cooling the composite plate, the thermal stresses will be accommodated by viscous flow of the glassy phase which permeates the structure. Thereafter, when the glass transition temperature is reached and the glass solidifies, stresses will build up in the crystalline phase to produce the observed lattice strains. The matrix was, however, sufficiently strong and free from defects to resist cracking. This is in contrast to findings on Pyrex matrix composites [12] where the thermal mismatch

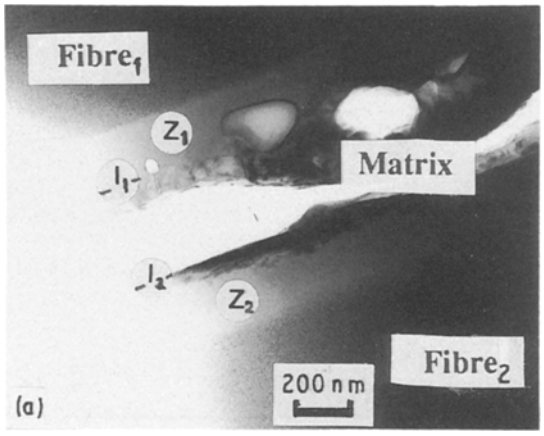

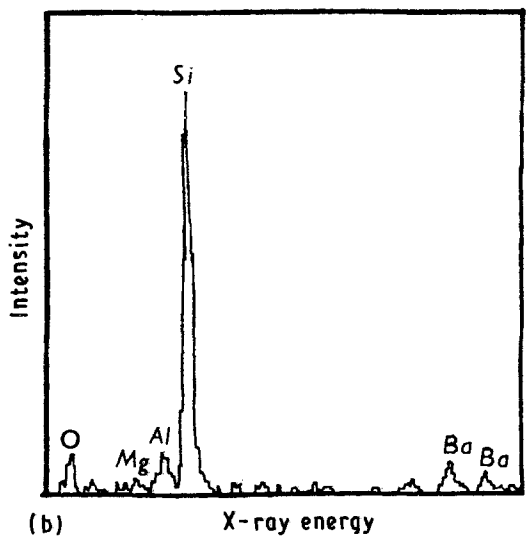

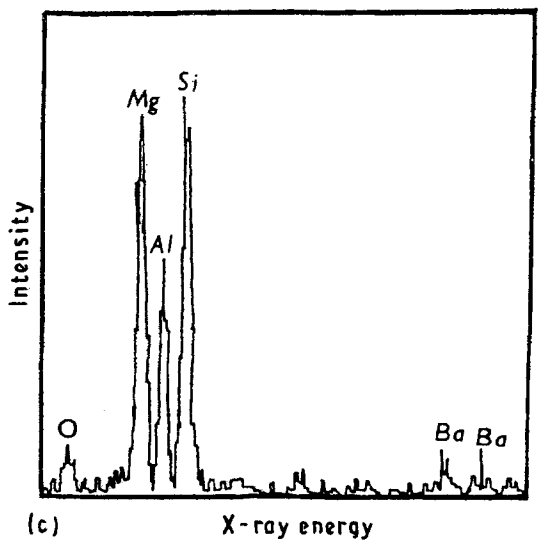

Figure 15 (a) 1100 °C HT plate, fibre/matrix interface, TEM. (b) Interface zone, EDS. (c) Adjacent matrix, EDS.

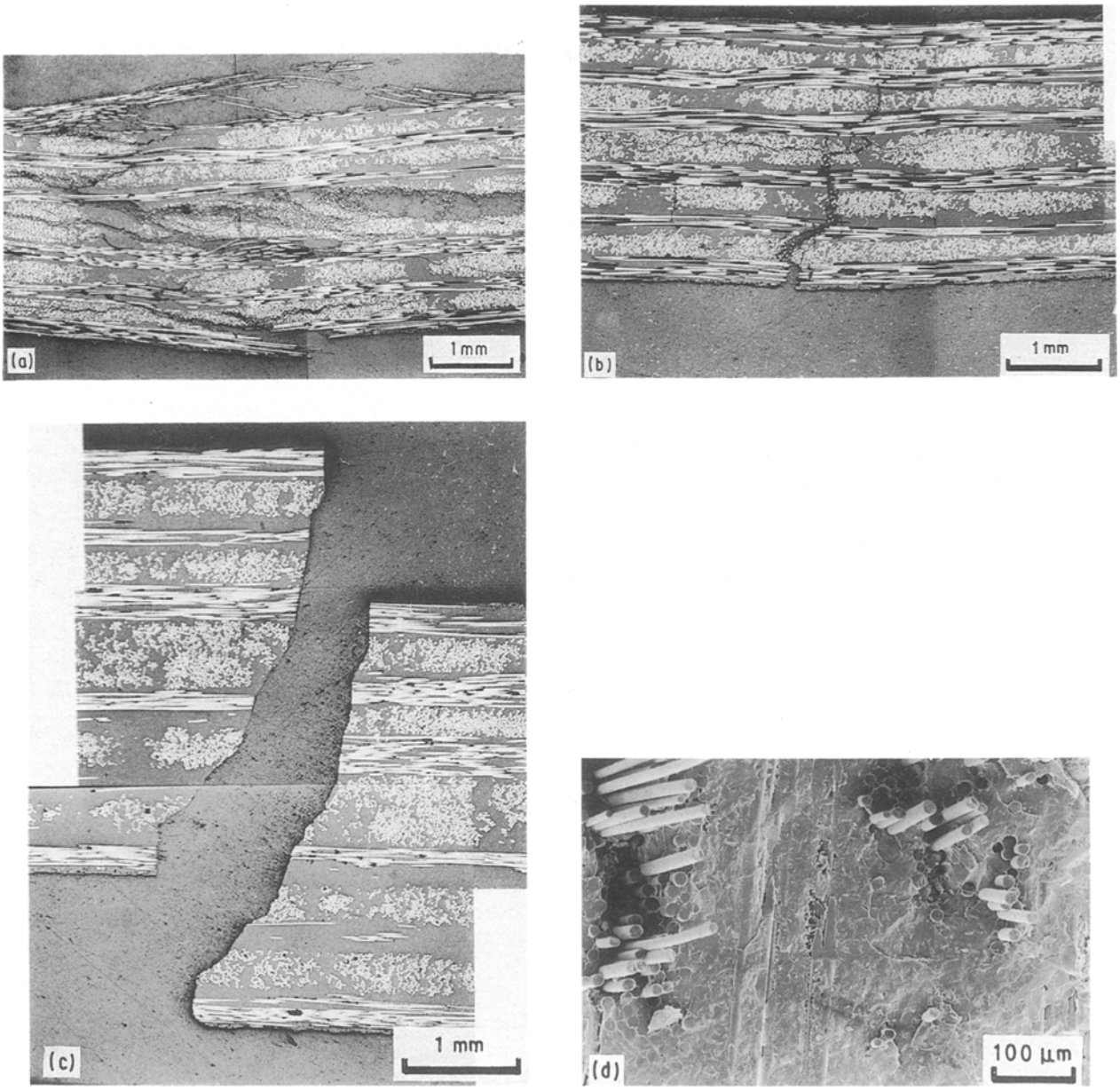

Figure 16 Optical micrographs of (a) 600 °C HT cross-ply plate, (b) 800 °C HT cross-ply plate, (c) 1000 °C HT cross-ply plate, all polished sections through fracture, and (d) scanning electron micrograph of a 1100 °C HT cross-ply plate, fracture surface.

between Pyrex ($3.2 \times 10^{-6}\,K^{-1}$) and the cristobalite phase which was present ($27 \times 10^{-6}\,K^{-1}$) led to very severe microcracking upon cooling the composite from the manufacturing temperature, in this case $\sim 950\,°C$.

The presence in the matrix of mullite and hexacelsian was not, however, unexpected because local compositional variations would encourage their formation instead of the barium osumilite form of aluminosilicate; some segregation of barium and magnesium would have a major influence in this respect. Indeed, such variations evidently occur on a very localized scale, as indicated by the proximity of particles of mullite and hexacelsian, each less than 1 µm in size, see Fig. 9a. The respective phase relationships are indicated in the phase diagram, Fig. 18, where mullite (AS) and hexacelsian (BAS) are seen to have adjacent phase fields.

With regard to the glassy regions, the large amount present of these remnants of crystallization suggests that either the matrix composition of the original glass had not been optimized, or the nucleating agent had not been fully effective. Indeed, no nucleating agent was located although it is known that 0.7 wt % As_2O_3 had been added to the matrix in order to inhibit oxidation of the Nicalon fibres. The failure to detect any arsenic using the EDS system may be due to the close proximity of the arsenic *L* X-ray lines to *K* lines from the other elements (magnesium, aluminium and silicon) rendering such a small amount of arsenic difficult to detect.

Studies of the fibre/matrix interface showed that a chemical reaction had taken place there during manufacture of the composite plate. The reaction zone, which was ~ 50 nm thick, was enriched in carbon, somewhat similar to the interfaces reported in other glass ceramics reinforced with Nicalon fibres, such as lithium aluminosilicate [13, 14] and calcium aluminosilicate systems. Cooper and Chyung [15] who produced TEM lattice images of the graphitic interface,

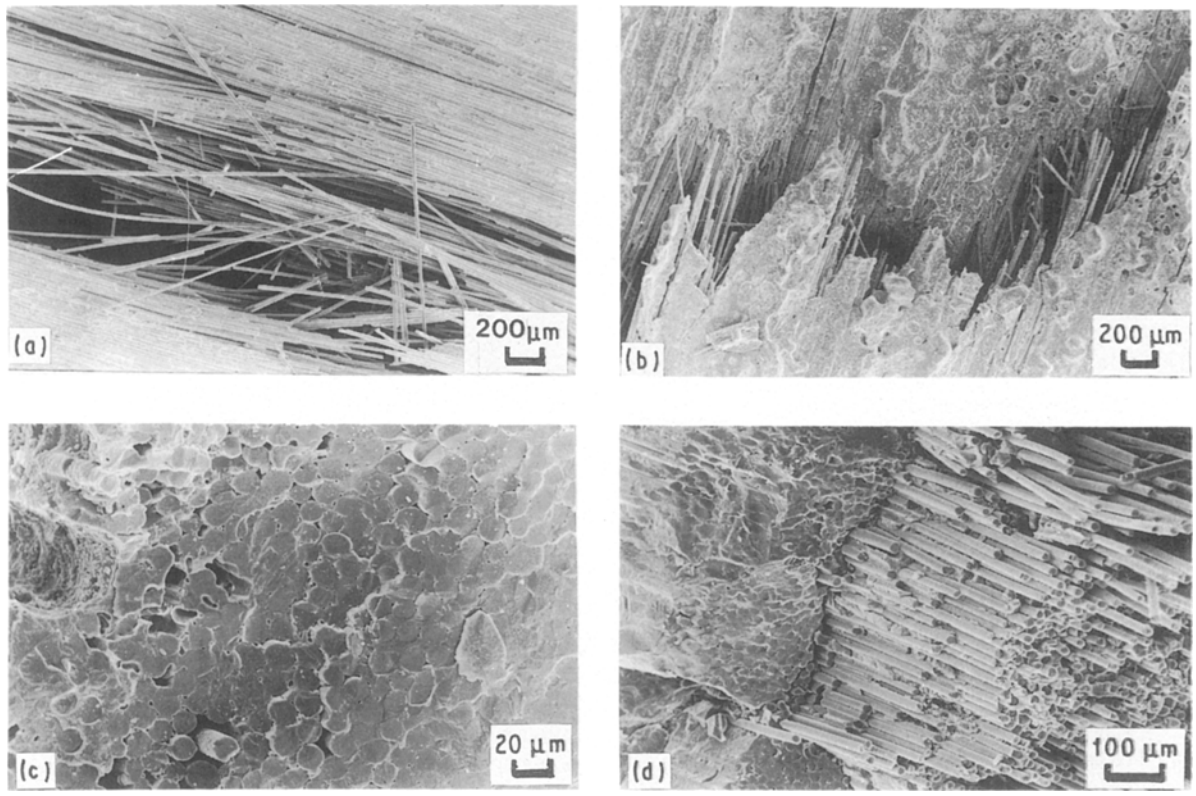

Figure 17 Scanning electron micrographs of (a) 600 °C HT, (b) 800 °C HT, (c) 1000 °C HT and (d) 1100 °C HT unidirectional plates, fracture surface.

TABLE IV Compositions (wt %) of matrix phases

	O	Mg	Al	Si	Ba	± 5 vol %
Barium osumilite (matrix)	44.4	4.5	15.0	23.4	12.7	~ 60
Hexacelsian (lighter phase)	34.0	–	14.4	15.0	36.6	~ 20
Mullite (darker phase)	48.8	–	38.0	13.2	–	~ 10
Glass (silica rich)	–	~ 1	~ 2		~ 5	~ 10

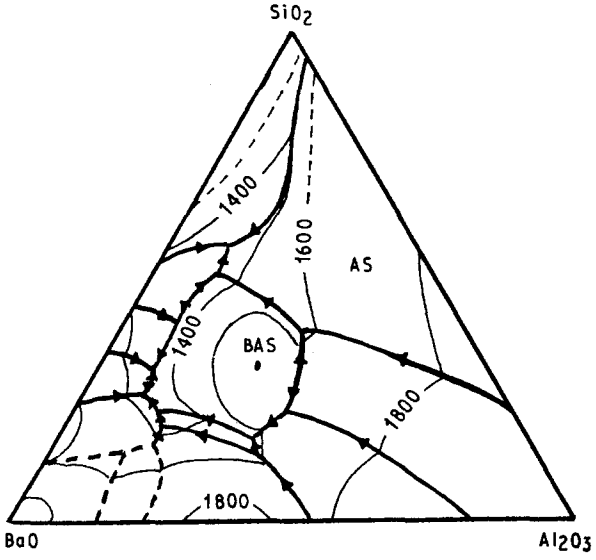

Figure 18 The $BaO–Al_2O_3–SiO_2$ ternary phase diagram.

proposed the following reaction based upon the interaction between the silicon carbide component of the Nicalon fibre and the oxygen present in the aluminosilicate

$$SiC_{(s)} + O_{2(g)} \rightarrow SiO_{2(s)} + C_{(s)}. \quad (1)$$

The carbon-rich reaction zone seen in the present work is much more developed than that described in earlier work on the Nicalon/Pyrex system [12], where the carbon-rich zone was no more than ~ 5 nm thick and in some batches of material was not found at all. The differences are attributable to fabrication factors, a high temperature (~ 1200 °C) being used to produce the barium osumilite-based composite compared with ~ 950 °C for Pyrex-based material. Both composite systems showed penetration of matrix elements into the Nicalon fibre: sodium, potassium and calcium from the Pyrex and barium, magnesium and aluminium from the aluminosilicate structure. Elemental concentrations were fairly small, a few per cent or less, with a penetration distance of some 100–200 nm in Pyrex/Nicalon and ~ 1–2 μm in barium osumilite/Nicalon, data which reflect the relatively higher mobilities of diffusing ions at the higher fabrication temperature used for barium osumilite/Nicalon.

Concerning the strength of the composite, application of the rule of mixtures principle would give a predicted value of ~ 1 GPa. This calculation assumes a tensile strength of 2.8 GPa (Nippon Carbon Data) for Nicalon fibre, ~ 100 MPa for the matrix ceramic, and a fibre volume fraction of 0.4. The measured flexural strength was, however, only 320 ± 80 MPa for as-received plate, well below this value, especially

when one considers that quoted flexural strengths are some one and a half times greater than tensile strengths. This would, nevertheless, appear to indicate a somewhat better product than that tested by Mandell *et al.* [7] with its tensile strength of 225 MPa, although the plate used for testing of heat-treated specimens, which gave an initial value of 260 $\pm$ 30 MPa, did not compare so favourably.

The low strength is not believed to be primarily due to a poor quality matrix. It was multi-phased but there was no strong evidence to suggest that any of the phases was a major source of mechanical failure; neither did the pores produced during manufacture appear to initiate fracture or to constitute a source of weakness. Evidence was, however, available showing that the fibres themselves had been mechanically degraded during manufacture as a result of chemical attack although this decrease, to approximately one-half the original value, would not account fully for the low recorded strength of the composite. Considering next the strength of the bond between fibre and matrix, the indentation test revealed a relatively low interfacial shear strength whilst the mechanical test was characterized by extensive fibre pull-out. Such interface behaviour was not dissimilar to that reported on calcium aluminosilicate/Nicalon [15] and lithium aluminosilicate/Nicalon [13, 14], where the composite properties are also essentially interface controlled. Hence, whilst a high strength is not achieved, the material is not brittle but exhibits some degree of toughness as demonstrated by the controlled mode of failure, at least in that part of the composite plate subject to tensile forces. The more complex stress situation in other regions of the composite such as the compressive face led to substantial delamination, possibly arising from matrix fragmentation followed by fibre buckling initiated at the poorly consolidated surface.

The cross-ply plate also exhibited delamination, mainly in the 90° plies, with the 0° plies failing by fibre pull-out. Nevertheless, the measured flexural strength, $\sim 250 \pm 30$ MPa, was similar to that recorded for unidirectional material, despite the fact that it had only half as many fibres aligned to support the applied tensile load. Hence, it may be suggested that the cross-ply plate had fared better with respect to rule-of-mixtures predictions, taking into account the complex stress situation associated with the flexural mode of testing.

4.2. Effect of heat treatment

Exposure of the composites to oxidizing environments at high temperature caused a number of microstructural changes. These were not detectable by XRD which suggested that the nature and proportions of the crystalline matrix phases were unaffected by heating, even at 1100 °C for 60 h. Optical microscopy on polished sections showed, however, that voids up to 50 μm in size had formed in the matrix at this temperature. Such voids were shown to be associated with some exudation of the glassy phase, accompanied by entrapped crystalline particles, due to expansion of the surrounding solid crystalline matrix components. The fact that most of the glass was expelled from the lower face of the specimen suggests a gravitational contribution to the direction of flow.

The changes incurred by heat treatment were apparent at the interface after 60 h at 800 °C when the carbon-rich reaction layer showed voids at the interface and "bridges" of material between fibre and matrix. The extent of the interface reaction increased with temperature and after exposure at 1100 °C had thickened to $\sim$ 250 nm. At this stage the carbon enrichment had essentially disappeared to leave a comparatively featureless interface zone containing the elements oxygen and silicon. These data lead to the proposition that silica had formed as a result of fibre oxidation according to

$$SiC_{(s)} + 2O_{2(g)} \rightarrow CO_{2(g)} \text{ or } CO_{(g)} \quad (2)$$

and that the carbon-rich interface has oxidized

$$C_{(s)} + O_{2(g)} \rightarrow CO_{2(g)} \text{ or } CO_{(g)} \quad (3)$$

Thus the gaseous nature of products in both reactions would account for the presence of voids at the interface. It also appears that, at 1100 °C, magnesium ions have diffused into the adjacent matrix at the same time as the silica was forming in the outer layers of the fibre.

The fibre/matrix interface friction stress showed a small increase to 8 $\pm$ 2 MPa after the 800 °C exposure, consistent with silica "bridges" starting to develop between fibre and matrix. This change in interface microstructure was accompanied by the development in the composite of a more brittle failure mode. The length of fibre pull-out was less and in the unidirectional material delamination was again a contributory factor as regards its inability to achieve anything like the strength predicted for an ideal composite.

The more extensive change in interface microstructure after treatment at 1000 °C was reflected in the interfacial friction stress, which had increased to $\sim 40 \pm 20$ MPa. The development there of a stronger bond between fibre and matrix resulted in little interface sliding, with the result that a propagating crack was no longer deflected around a fibre. As a consequence, brittle failure took place, leading to the characteristic planar fracture surfaces. Because the fibres were then breaking in a brittle fashion well below their load-bearing capability, even allowing for a degradation in strength due to a surface reaction as discussed above, the measured strengths were now much lower, $\sim 120 \pm 30$ and $\sim 80 \pm 30$ MPa for unidirectional and cross-ply plate, respectively. These data on heat-treatment effects on structure and properties of the composite material lead us to reaffirm our contention that the mechanical properties are controlled by the carbon at the interface and that the matrix is, in these materials, of secondary importance. The last part of the puzzle can now be put in place, the differences noted between the interior and exterior regions of the composite plates.

Structurally, the interface observed in samples heated to 1100 °C resembled that above, with some thickening of the silica layer. Interfacial friction

stresses at the edge increased to $\sim 80 \pm 15$ and $\sim 50 \pm 10$ MPa for unidirectional and cross-ply samples, respectively, but brittle fracture was observed only at the edges of the samples, and in the 90° plies of the cross-ply, with pull-out observed in the 0° plies. The occurrence of pull-out produced a controlled mode of fracture in both cases, but whereas a high value of flexural strength (~ 230 MPa) was seen for unidirectional material that of the cross-ply remained low at ~ 85 MPa.

The only major difference between the 1100 °C and 1000 °C heated samples is the flow of a glassy phase that occurs above 1000 °C. It is thought that the outward flow of the glassy phase may have counteracted the ingress of oxidizing gases, and sealed porosity which may act as a transport route to the sample interior for gases. As a consequence, fibres in the centre of the sample were not exposed to oxidizing conditions and preserved a weak interface which permitted fibre pull-out. Oxidation can still proceed by other mechanisms, such as "wicking" along the fibre/matrix interface from exposed fibre ends as seen in Pyrex/carbon material [16], which would explain why brittle failure occurs in 90° plies in the cross-ply, where the two exposed ends of the fibre are only 10 mm apart. Similar attack occurs at the end of the 0° plies, but evidently after 60 h the attack has not proceeded far enough to reach the centre of the sample. The polished section used to determine interface friction stress was taken from the end of the test specimen, where "wicking" has occurred, which would explain why no significant difference was found between surface and interior fibres for the cross-ply, when it is expected that fibres in the interior have much weaker fibre/matrix bonds. A difference was seen in the unidirectional plate where interfacial friction stresses in the interior of a polished section from the centre of the 1100 °C heated plate showed no change from the as-received value, while values at the edge were $\sim 80 \pm 10$ MPa.

5. Conclusions

Barium osumilite glass-ceramics reinforced with Nicalon have been shown to possess a four-phase matrix consisting of barium osumilite, hexacelsian, mullite and a silica-rich glassy phase. The presence of so many phases in the matrix is undesirable as thermal mismatch sets up strains in the matrix. At high temperatures, the load-bearing capability of the matrix is limited by flow of the glassy phase between 1000 and 1100 °C, leaving voids in the matrix which may act as flaws and reduce the load-bearing volume of the matrix. A short-term benefit derived from matrix flow is the sealing of surface porosity which affords some protection for core fibres against oxidation.

The changes in the matrix do not, however, play a major role in determining composite properties, which are controlled by the fibre/matrix interface. A change in interface microstructure from a weak carbon-rich interface to one where the fibre and matrix are strongly bonded together by a silica layer is reflected in a significant increase in interfacial friction stress and a change from fibre pull-out and delamination at the fracture surface to a planar brittle failure. The flexural strength of the composite system decreases with increasing bond strength although an increase in strength is seen for 1100 °C aged samples which have unoxidized fibres capable of pull-out in the interior.

Evidently if barium osumilite is to be used effectively as a matrix material, fabrication routes need to be devised which eliminate undesirable second phases, in particular the glass. Methods of protecting the fibre/matrix interface from oxidation also require investigation, as formation of a strong fibre/matrix bond by oxidation leads to a catastrophic brittle failure mode in the composite.

Acknowledgements

The authors acknowledge the financial support of Rolls-Royce plc, RAE Pyestock, and the SERC, and thank Rev. B. Chapman for assistance with XRD studies.

References

1. R. A. J. SAMBELL, A. BRIGGS, D. C. PHILLIPS and D. H. BOWEN, *J. Mater. Sci.* 7 (1972) 676.
2. K. M. PREWO and J. J. BRENNAN, *ibid.* **17** (1982) 1201.
3. K. M. PREWO, *ibid.* **21** (1986) 3590.
4. J. J. BRENNAN, K. CHYUNG and P. M. TAYLOR, US Pat no. 4589900 May 20 (1986).
5. K. P. GADKAREE and K. CHYUNG, *Amer. Ceram. Soc. Bull.* **65** (1986) 370.
6. L. F. JOHNSON, D. P. H. HASSELMAN and K. CHYUNG, *J. Amer. Ceram. Soc.* **70** (1987) C135
7. J. F. MANDELL, D. H. GRANDE and J. JACOBS, *J. Eng. Gas. Turb. Power. Trans. ASME* **109** (1987) 267.
8. D. B. MARSHALL and A. G. EVANS, *J. Amer. Ceram. Soc.* **68** (1985) 225.
9. E. GUGEL, H. VOGEL and O. OSTERRLED, *Ber. Deut. Keram. Ges.* **41** (1964) 520.
10. Y. TAKEUCHI, *Mineral J. (Jpn)* **2** (1958) 311.
11. National Bureau of Standards (US) Monograph **25** Sec. 3 (1964).
12. S. M. BLEAY and V. D. SCOTT, *J. Mater. Sci.* **26** (1991) 2229.
13. R. CHAIN and R. H. HEUER, *Adv. Ceram. Mater.* **2** (1987) 154.
14. E. BISCHOFF, M. RÜHLE, O. SBAIZERO and A. G. EVANS, *J. Amer. Ceram. Soc.* **72** (1989) 741
15. R. F. COOPER and K. CHYUNG, *J. Mater. Sci.* **22** (1987) 3148.
16. S. M. BLEAY and V. D. SCOTT, *ibid.* **26** (1991) 3544.

Received 4 April
and accepted 1 May 1991